Cells and Materials

Volume 9 | Number 1 Article 4

1999

Mechanical Properties of Dendritic Pd-Cu-Ga Dental Alloys

Efstratios Papazoglou
The Ohio State University

Qiang Wu
The Ohio State University

William A. Brantley
The Ohio State University

John C. Mitchell
The Ohio State University

Glyn Meyrick
The Ohio State University

Cells and Materials Vol. 9, No. 1, 1999 (pages 43-54) 1051-6794/99$5.00+.25
Scanning Microscopy International, Chicago (AMF O'Hare), IL 60666 USA

MECHANICAL PROPERTIES OF DENDRITIC Pd-Cu-Ga DENTAL ALLOYS

Efstratios Papazoglou,[1] Qiang Wu,[1,4] William A. Brantley,[1,*] John C. Mitchell,[2] and Glyn Meyrick[3]

[1]College of Dentistry, [2]Department of Geological Sciences, [3]Department of Materials Science and Engineering
The Ohio State University, Columbus, OH 43210

[4]Present address: Therm-O-Disc, Inc., Mansfield, OH 44907

(Received for publication May 5, 1998 and in revised form October 18, 1998)

Abstract

Three Pd-Cu-Ga dental alloys with very similar nominal compositions and dendritic as-cast microstructures were selected for study: Option (Ney Dental) and Spartan (Williams/Ivoclar) contain a small amount of boron, while Spartan Plus (Williams/Ivoclar) is boron-free. Bars of each alloy were tested in tension for the as-cast and simulated porcelain-firing conditions, and values of mechanical properties were measured. Fracture surfaces and microstructures of axially sectioned and etched fracture specimens were observed with the scanning electron microscope (SEM). Except for the elastic modulus, significant differences were typically found in alloy properties. Heat treatment eliminated the dendritic microstructure, decreased strength and increased ductility. Values of mechanical properties depend on the presence (orientation and distribution) of dendrites but not boron content. The amounts of casting porosity in the samples were too small to affect their mechanical properties significantly.

Key Words: Palladium, dental alloy, microstructure, dendrite, scanning electron microscopy, tension test, mechanical properties.

*Address for Correspondence:
William A. Brantley
Section of Restorative Dentistry, Prosthodontics and Endodontics
College of Dentistry
Ohio State University
305 West 12th Avenue
Columbus, Ohio 43210-1241
Telephone number: (614) 292-0773
FAX number: (614) 292-9422
E-mail: brantley.1@osu.edu or wbrantle@columbus.rr.com

Introduction

The Pd-Cu-Ga alloys containing about 10 weight percent (wt%) Cu and 6-9 wt% Ga date from the patent by Schaffer (1983) for the alloy Option (Ney Dental, Bloomfield, CT). This alloy became commercially successful and stimulated development efforts by other manufacturers (Vrijhoef and Greener, 1988) for a series of alloys with Option-like compositions such as the alloys Spartan and Spartan Plus (Williams/Ivoclar, Amherst, NY). These alloys are used for metal-ceramic restorations (Carr and Brantley, 1991), implant-supported prostheses (Stewart *et al.*, 1992) and potentially for removable partial denture frameworks (Asgar, 1988). This group of Pd-Cu-Ga alloys lacks grain-refining elements (typically ruthenium) and has a dendritic as-cast structure (Brantley *et al.*, 1993). The dendritic Pd-Cu-Ga alloys remain popular clinically, particularly for implant-supported prosthesis applications where their relatively high values of elastic modulus and yield strength provide excellent flexural rigidity for long-span restorations.

The effect of heat treatment (as-cast versus simulated porcelain firing) on the hardness of these alloys has been previously studied (Carr *et al.*, 1993; Brantley *et al.*, 1996, 1998). It was the purpose of this investigation to determine a wider variety of mechanical properties for alloys cast under standard dental laboratory conditions and to compare these findings to the previous hardness measurements. Additionally, the effect of heat treatment simulating porcelain firing cycles on the mechanical properties was investigated.

Materials and Methods

Three Pd-Cu-Ga alloys with the nominal composition of 79Pd-10Cu-9Ga-2Au (wt%) and dendritic as-cast microstructures were selected for study: Option and Spartan contain a very small amount of boron; Spartan Plus is boron-free according to the manufacturer.

Bars of each alloy were tested in tension for the as-cast and simulated porcelain-firing conditions. Polystyrene plastic patterns (Salco, Romeoville, IL) of

approximately 3 mm diameter, which satisfy the dimensional requirements in ADA specifications nos. 5 (1996) and 38 (1991), were used to prepare cast specimens for tensile testing. Each specimen was sprued in a horizontal configuration, because horizontal spruing produces less porous tensile specimens than vertical spruing (Asgar *et al.*, 1969). Each pattern was invested in a separate casting ring, using a carbon-free, phosphate-bonded investment (Cera-Fina, Whip-Mix, Louisville, KY). A two-stage burn-out procedure with a peak temperature of 815°C (1,500°F) was employed. Melting was accomplished using a torch with approximately 35 Pa gas (bottled liquid petroleum) and 70 Pa oxygen pressures (as recommended in the Williams/Ivoclar product information literature). Centrifugal casting was performed in air with a broken-arm casting machine (Kerr/Sybron, Romulus, MI). Each alloy was melted in a separate ceramic crucible. Six specimens of each alloy were cast for each condition (as-cast or heat-treated), all from the same batch, and all castings were bench-cooled. After devesting, sprues were cut off with a carborundum separating disk, and any visible nodules and fins were carefully removed. The specimens were not air-abraded or polished. No specimens had visible shrinkage defects or porosities, and none was discarded. The as-cast groups did not receive any further treatment. The heat-treated groups were placed in a furnace and fired according the recommended cycles for Vita VMK 69 porcelain (Vident, Baldwin Park, CA). The firing cycles for the opaque porcelain, body porcelain and glaze have been published (Papazoglou *et al.*, 1993), and each cycle involved heating the alloy in a temperature range from approximately 650°C to over 900°C during an 8-10 minute period.

The initial diameter for each tensile test bar was measured with a digital micrometer (Mitutoyo, Shiwa, Japan), and the central gauge section of 15 mm length for the determination of percentage elongation was marked with a sharp blade and measured with a traveling microscope (Measurescope MM-11, Nikon, Tokyo, Japan). All specimens were loaded by a screw-driven mechanical testing machine (Model 4204, Instron Corp., Canton, MA), using a crosshead speed of 0.5 mm/min. The interiors of two Jacobs chucks were custom-modified by a grinding procedure (Bridgeport *et al.*, 1993) to provide grips with self-aligning capability during tensile loading for the test bars (ASM, 1992). The specimen elongation was recorded over the central 10 mm length using a strain gage extensometer. The strain gage elongation, the load and the position of the crosshead were recorded by means of a personal computer (PC), using the software program LabVIEW (National Instruments, Austin, TX) for Windows and a data acquisition card. The values of the strain gage elongation, the load and the position of the crosshead were also observed during the experiment on the screen of the PC monitor in a graph form. Before the elongation reached 1 mm or 10%, the test was interrupted and the extensometer removed, because its maximum allowable elongation was 10%. Then the specimen was further loaded until fracture occurred. The raw data from each test bar were stored in the computer as a text file. The software program Excel (Microsoft Corp., Redmond, WA) was used to generate graphs of engineering stress versus strain from these data.

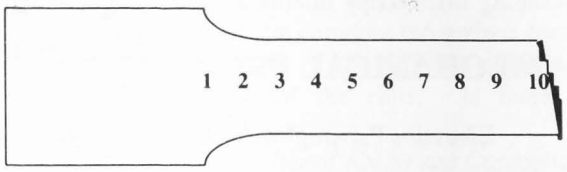

Figure 1. Location of porosity measurements on the sectioned half-bars.

The following formulas were used to derive engineering stress (s) and engineering strain (e):

$$s = P/A_o \tag{1}$$

$$e = \Delta l/l_o \tag{2}$$

where P is the load, A_o is the initial cross-section area, Δl is the change in gage length, l_o is the initial gage length, and $E = s/e$ is the Young's modulus in the elastic region. The ADA specification No. 5 for dental casting alloys (1996) requires the calculation of the 0.1% yield strength (0.1% *YS*), while the ADA specification no. 38 for metal-ceramic systems (1991) requires the measurement of the 0.2% yield strength (0.2% *YS*). These yield strengths were obtained from the points of intersection with the stress-strain curve of lines drawn parallel to the elastic portion of the curve, but displaced by $\Delta e = 0.001$ (0.1%) or 0.002 (0.2%), respectively. The ultimate tensile strength (UTS) is the maximum value of stress applied to the specimen.

The stress-strain curve of many ductile metals in the region of uniform plastic deformation can be described mathematically by a simple power-law relationship:

$$\sigma = K \epsilon^{n} \tag{3}$$

where n and K are constants known as the strain-hardening exponent and the strength coefficient, respectively (Dieter, 1986). Here σ and ϵ are the true stress (P/A) and true strain ($\Delta l/l$), respectively, where A and l are instantaneous values of the cross-section area and gage length, respectively. The values of true stress (σ) and strain (ϵ) used in the power-law relation were calculated from the engineering stress (s) and strain (e), using the

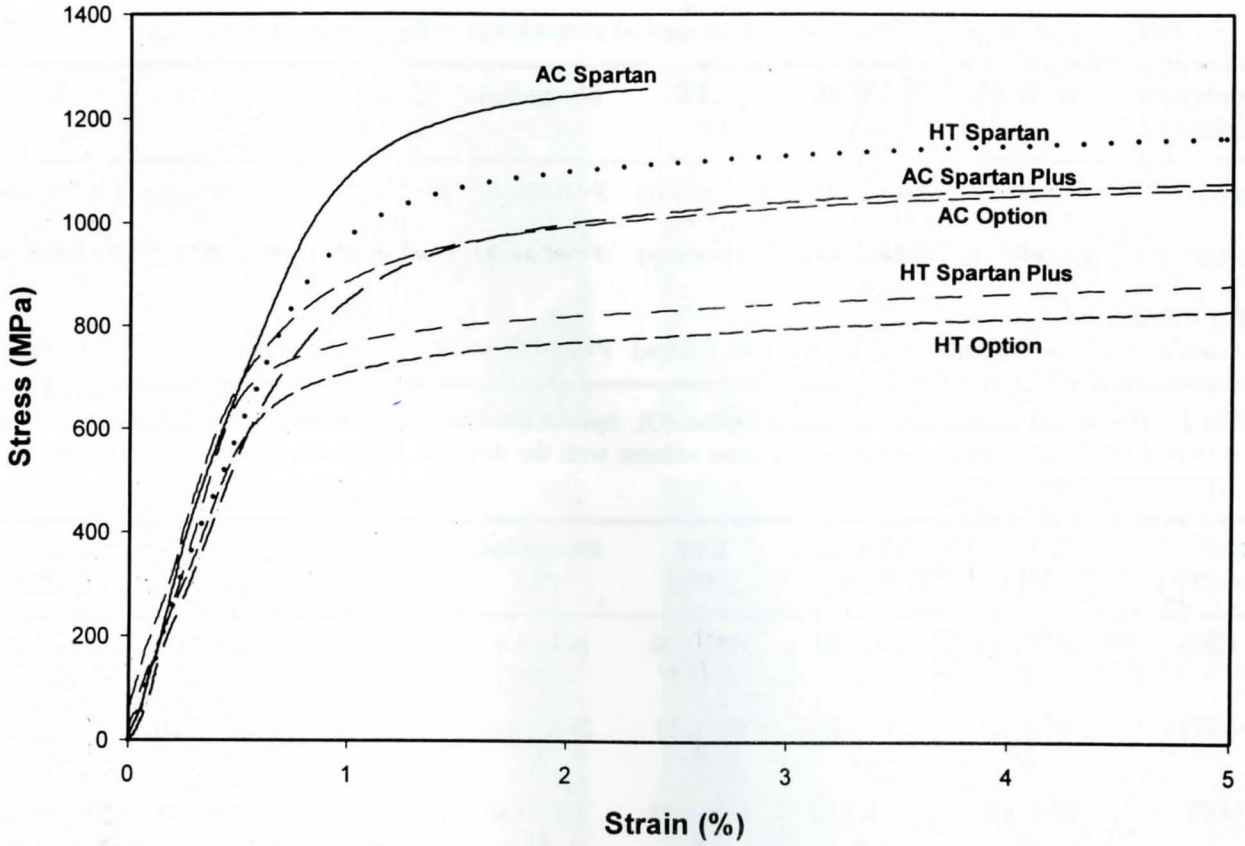

Figure 2. Representative engineering stress-strain curves for the three dendritic Pd-Cu-Ga alloys. The curve for the as-cast Spartan ended at the fracture point, while all the other curves were truncated at 5% strain.

following equations (Dieter, 1986):

$$\epsilon = \ln (1+e) \quad (4)$$

and

$$\sigma = s\,(1+e). \quad (5)$$

The constants n and K were found from the true stress-strain curve by taking logarithms of both sides of the power-law relation:

$$(ln\ \sigma) = n\ (ln\ \epsilon) + (ln\ K). \quad (6)$$

This is the equation of a straight line whose slope is n and intercept on the vertical axis is $(ln\ K)$. Once necking occurs, the power-law relationship, eq. (6), does not apply, since strains and stresses are no longer uniform over the gage length. The onset of necking occurs at the point of maximum load or engineering stress (i.e., UTS) and is readily observable on load-elongation curves or stress-strain curves. The strain-hardening exponent n was obtained from the region between the 0.1% YS and the UTS.

Fracture surfaces on each broken sample were examined with a JSM-820 (JEOL Ltd, Tokyo, Japan) scanning electron microscope (SEM). The objectives of the SEM observations were to assess the general metallurgical character (ductile or brittle) of tensile fracture, and to ascertain if porosity and other casting defects determined the original location of the fracture sites for the three high-palladium alloys investigated. SEM evidence was also sought on fracture surfaces for networks of microvoids similar to those for ductile fracture in wrought metals (Lausten *et al.*, 1993). Specimens were not cleaned ultrasonically before observation. After SEM examination, the percentage elongation was obtained from the measurement of permanent change in the gage length after carefully fitting together the two fractured portions of the specimen.

Mean values and standard deviations (SD) for each of the mechanical properties were determined. Two-way analysis of variance (ANOVA) and the Tukey-Kramer HSD test ($\alpha = 0.05$) were performed with a statistical software package (SPSS, Chicago, IL) to compare each of the mechanical properties for the three alloys in the as-cast and heat-treated conditions.

The smaller portions of the fractured test bars for each as-cast alloy were mounted in metallographic epoxide resin (Leco Corp., Saint Joseph, MI) and sectioned

Table 1. Two-way ANOVA results for mechanical properties (s = significant; ns = not significant).

Independent Variable	0.1% YS	0.2% YS	UTS	Elongation	E	n	K
Alloy	P<0.0001(s)	P<0.0001(s)	P<0.0001(s)	P<0.0001(s)	P=0.4953(ns)	P=0.1194(ns)	P<0.0001(s)
Condition	P<0.0001(s)	P<0.0001(s)	P<0.0001(s)	P<0.0001(s)	P=0.5229(ns)	P<0.0005(s)	P<0.0001(s)
*Alloy * Condition Interaction*	P=0.4751(ns)	P=0.3317(ns)	P=0.3603(ns)	P=0.0773(ns)	P=0.3205(ns)	P=0.1365(ns)	P=0.488(ns)

Table 2. Mechanical properties of the alloys Option (O), Spartan (S) and Spartan Plus (SP), in the as-cast (AC) and heat-treated (HT) conditions. Groups in the same column with the different letters are significantly different ($P < 0.05$).

Alloy/ Condition	0.1% YS (MPa)	0.2% YS (MPa)	UTS (MPa)	Elongation (%)	E (GPa)	n	K (MPa)
O (AC)	817±82 C	870±60 C	1072±26 C	6.9±2.5 CD	136±21 A	0.13±0.03 AB	1699 ± 174 B
O (HT)	679±21 D	706±22 D	957±23 D	25.1±2.1 A	119±16 A	0.11±0.00 B	1241±36 C
S (AC)	1070±64 A	1120±50 A	1259±32 A	2.7±1.0 D	131±24 A	0.18±0.06 A	2552±517 A
S (HT)	954±35 B	998±27 B	1161±18 B	14.9±3.5 B	127±17 A	0.11±0.01 B	1718±45 B
SP (AC)	791±29 C	851±31 C	1075±71 C	8.7±4.8 C	133±15 A	0.14±0.03 AB	1773±271 B
SP (HT)	700±13 D	725±9 D	1002±9 D	24.1±1.5 A	141±28 A	0.11±0.00 B	1271±16 C

Figures 3-8 on the facing page

Figure 3. Low-magnification scanning electron micrograph of the tensile fracture surface for an as-cast Option specimen. The dendritic microstructure is the source of an apparent web-like constituent, when the fracture surface is viewed at low magnification. Bar = 100 μm.

Figure 4. High-magnification scanning electron micrograph of the tensile fracture surface for an as-cast Option specimen in which dimples (D) and ridges (R) of the web-like constituent (Fig. 3) can be seen. Bar = 10 μm.

Figure 5. Scanning electron micrograph of the tensile fracture surface for an as-cast Spartan specimen. Fracture across several parallel dendrites can be seen. Bar = 10 μm.

Figure 6. High-magnification scanning electron micrograph of the tensile fracture surface for an as-cast Spartan specimen. The apparent lamellar structure suggests fracture through an interdendritic region. A relatively large pore (P) with terraced sides can be seen at the lower left edge of the micrograph. Bar = 10 μm.

Figure 7. Scanning electron micrograph of the tensile fracture surface for a heat-treated Spartan Plus specimen. The surface is dominated by dimples (D) and contains many small pores (some indicated by P). Bar = 10 μm.

Figure 8. Scanning electron micrograph of the tensile fracture surface for a heat-treated Option specimen. The surface shows a preponderance of dimples and contains a large pore which may have a pivotal role for fracture. Bar = 10 μm.

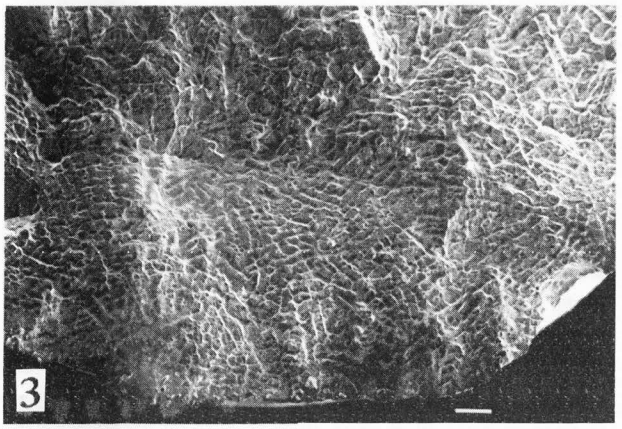

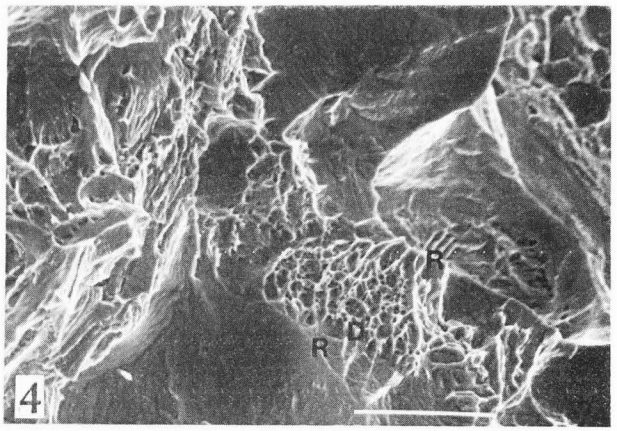

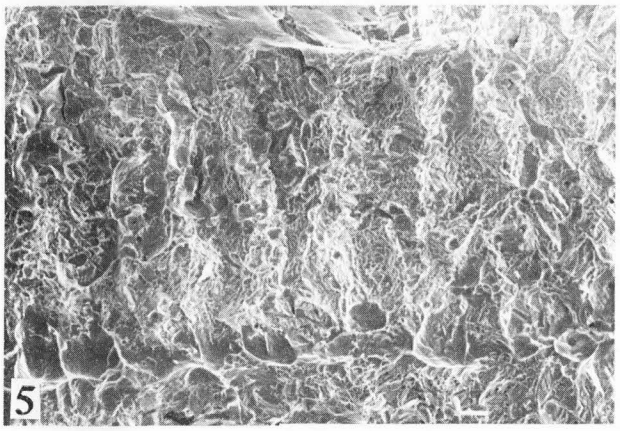

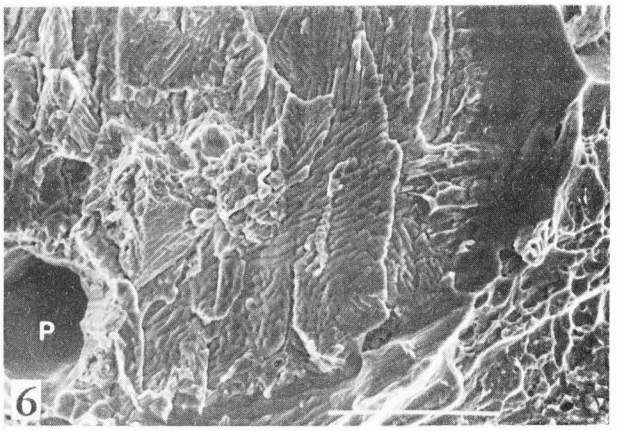

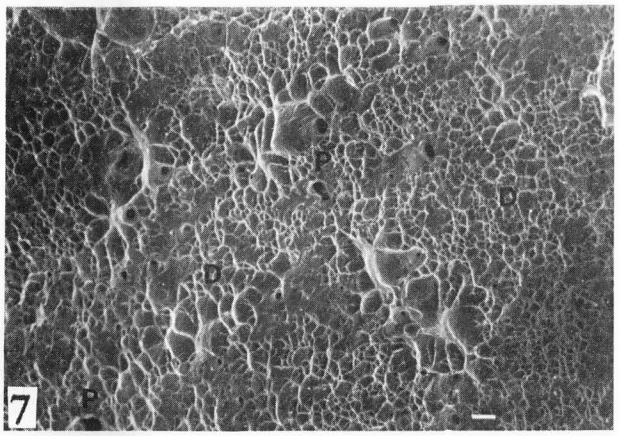

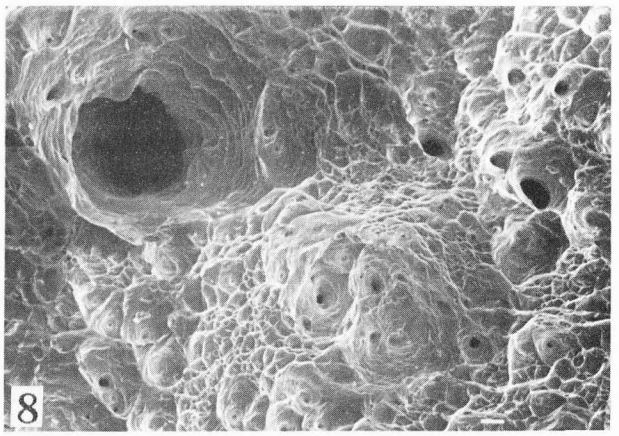

parallel to the axis, using a slow-speed water-cooled diamond saw (Vari/Cut VC-50, Leco Corp.). After standard metallographic grinding and polishing through 0.05 μm alumina slurries, the cross-sections were examined in an optical microscope at X50 magnification for the presence of porosity and other casting defects. Quantitative metallographic techniques (Vander Voort, 1984) using computerized image analysis software (Omnimet® 4, Buehler Corp., Lake Bluff, IL) were employed to analyze the porosity in the test bars. The analysis routines included image acquisition, gray image enhancement (delineation), binarization (thresholding) and finally area measurement. Ten measurements were made from near the fracture site to near the gripped end for each test specimen (Fig. 1). The representative images of porosity were saved on a computer disk. To determine if the UTS for each alloy could be predicted by the total amount of porosity, the results were subjected to analysis of covariance using the statistical program JMP IN (SAS Institute, Cary, NC). The UTS was the dependent variable; the total porosity was the covariate, and the alloy type was the independent variable.

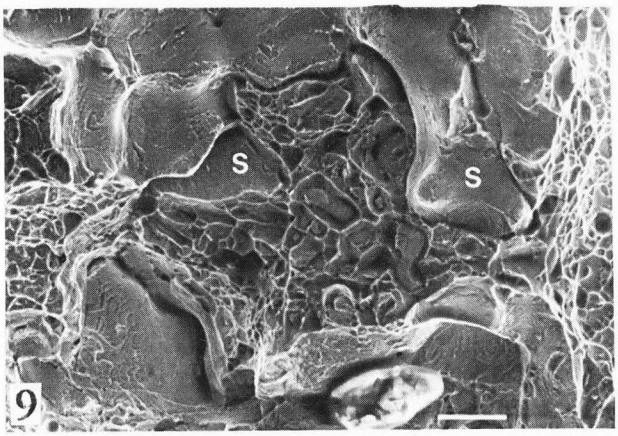

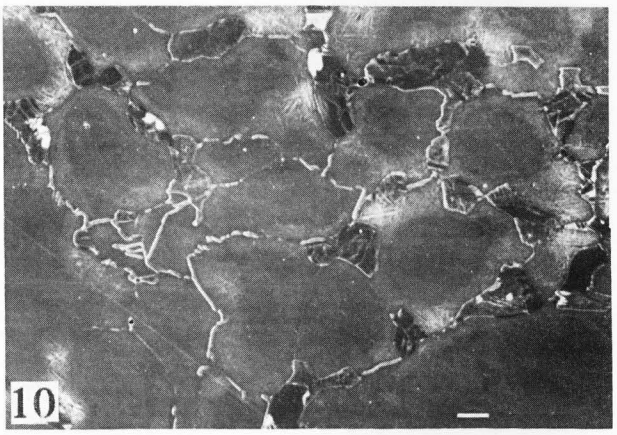

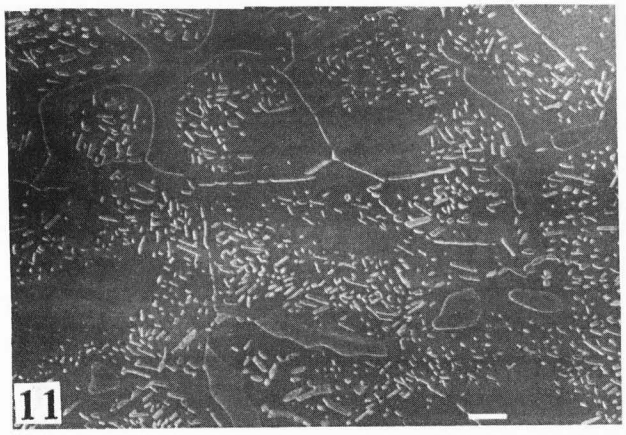

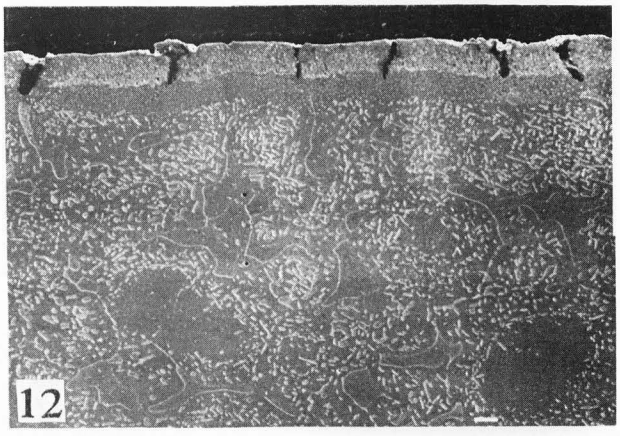

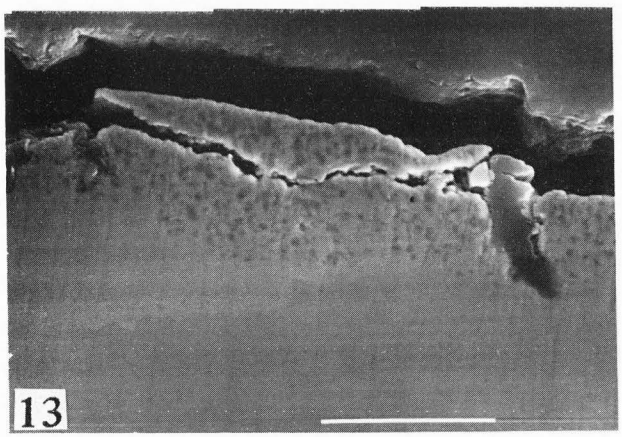

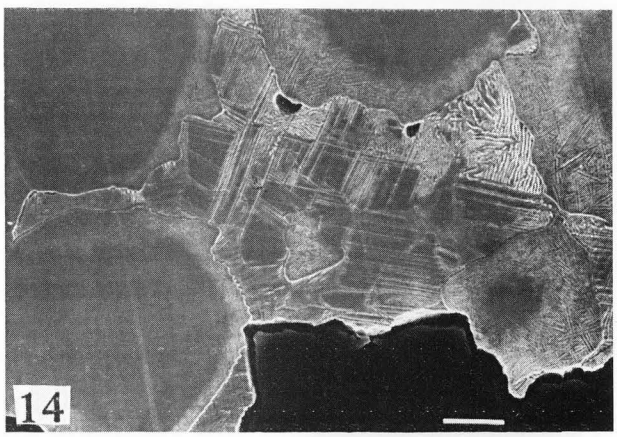

Finally, the polished cross-sections of fractured as-cast and heat-treated tension test bars were etched at room temperature with aqua regia and observed with the SEM to reveal the relationship between microstructure and nature of fracture.

Results

Representative engineering stress-strain curves of the three alloys in the as-cast and heat-treated conditions are shown in Figure 2. The results of the two-way ANOVA for each of the mechanical properties are presented in Table 1. It was found that there were significant differences in all mechanical properties of the three alloys for the as-cast and heat-treated conditions, except for E and n. Only E was not affected by either variable, whereas n depended significantly upon alloy condition. There was no interaction between alloy and condition.

Values (mean $\pm$ SD) of all mechanical properties are given in Table 2. The groups with the same letter that belong to the same column in Table 2 are not significantly different ($P > 0.05$). As noted already for

Figures 9-14 on the facing page

Figure 9. High-magnification scanning electron micrograph of the tensile fracture surface for a heat-treated Spartan specimen. The large secondary phase particles (S) are presumed to be Pd_2Ga, and smaller particles may be Pd_2Ga or a phase having a different Pd:Ga ratio. Bar = 10 μm.

Figure 10. Scanning electron micrograph of the polished and etched, sectioned surface for an as-cast Option specimen. The complex secondary phase in the interdendritic areas is evident. At this magnification, the microstructure somewhat resembles an equiaxed grain structure, instead of the dendritic structure seen at lower magnification (Fig. 3). Bar = 10 μm.

Figure 11. Scanning electron micrograph of the polished and etched, sectioned surface for a heat-treated Option specimen. The grain boundary structure and two different sizes of precipitates are visible. The original residual dendritic structure is suggested by the pattern formed by these precipitates. Bar = 10 μm.

Figure 12. Scanning electron micrograph of the polished and etched, sectioned surface for a heat-treated Option specimen. The microstructure of the near-surface area of a fractured tensile bar is shown. There is an outer subsurface oxidation region with some equidistant cracks that are perpendicular to the direction of tensile loading. The mounting resin has penetrated into these cracks, which terminate at a precipitate-free denuded zone. Bar = 10 μm.

Figure 13. High-magnification scanning electron micrograph of the polished sectioned surface for a heat-treated Spartan Plus specimen. A place where fracture in the subsurface oxidation region was parallel to the specimen axis is shown. Bar = 10 μm.

Figure 14. High magnification scanning electron micrograph of the polished and etched, sectioned surface for an as-cast Spartan Plus specimen. The lamellar eutectic and pronounced linear features suggestive of twinning are evident in the interdendritic region. Bar = 10 μm.

Table 1, except for E, significant differences were found in mechanical properties for the different alloys and conditions. For 0.1% YS, 0.2% YS and UTS, as-cast Spartan had the highest values, followed by the same alloy in the heat-treated condition. As-cast Option and as-cast Spartan Plus were not significantly different for these properties, and were stronger than heat-treated Option and heat-treated Spartan Plus, which were not significantly different from each other. The weakest alloys, heat-treated Option and Spartan Plus, had the highest permanent elongation at fracture. The lowest mean percentage elongation was found for the strongest alloy, as-cast Spartan, but this was not significantly different from the mean elongation for as-cast Option. Heat treatment significantly lowered the mean value of K for all three alloys, but the mean value of n was significantly lowered only for Spartan.

SEM examination of the fracture surfaces of the three as-cast alloys revealed porosity and ample evidence of the dendritic microstructure (Figs. 3, 4, 5 and 6). An apparent "web-like" pattern observed on the fracture surface of as-cast Option and Spartan Plus was not evident for as-cast Spartan, which had a lower percentage elongation at fracture. In general, the fracture for all three alloys appeared to have propagated preferentially through the interdendritic regions. Some regions containing dimples were observed. These are indicative of ductile fracture by microvoid coalescence (Dieter, 1986). Presumably, this occurred in the palladium solid solution dendrites, because the interdendritic regions should undergo a more brittle mode of fracture. For all three alloys, the heat-treated specimens showed substantial ductile fracture, as evidenced by the dominant presence of microvoid dimples (Figs. 7 and 8). Precipitates were observed (Fig. 9), which had sizes and shapes that were very similar to the Pd_2Ga secondary phase previously found in heat-treated coping specimens (Brantley *et al.*, 1996, 1998). The possibility that some particles observed in the above specimens correspond to fracture through Widmanstätten precipitates previously observed in these as-cast alloys (Brantley *et al.*, 1993, 1996, 1998) is considered unlikely, since these needle-shaped precipitates are not observed in smaller castings after similar heat treatment.

The total porosity for as cast Option was 0.23%, while values of 0.22% and 0.11% were found for as-cast Spartan and Spartan Plus, respectively. Analysis of covariance showed that porosity was not a significant factor for the UTS ($P = 0.17$) of the alloys.

SEM examination of the polished and etched, sectioned specimens (Figs. 10 and 11) verified that the simulated porcelain-firing heat treatment eliminated the dendritic structure of the as-cast alloys (Brantley *et al.*, 1993). X-ray diffraction and X-ray energy-dispersive spectroscopic analyses performed during another study in our laboratory (Brantley *et al.*, 1998) suggest that the precipitates in the heat-treated alloys (Figs. 9 and 11) are Pd_2Ga and perhaps other phases with different Pd:Ga ratios. Table 2 shows that this heat treatment decreased strength (YS, UTS) and increased ductility (percentage elongation) of the alloys. While the values of mechanical properties for individual specimens evidently depended on the presence (orientation and distribution) of dendrites, the similar results for Option and Spartan

Table 3. Mechanical properties of the alloys Option (O), Spartan (S) and Spartan Plus (SP), for the as-cast (AC) and heat-treated (HT) conditions from other publications and product information literature.

Alloy/ Condition	0.1% YS (MPa)	0.2% YS (MPa)	UTS (MPa)	Elongation (%)	E (GPa)	Vickers Hardness
O (AC) *						348
O (HT) *						292
S (AC) *						349
S (HT) *						314
SP (AC) *						354
SP (HT) *						296
S (AC) §		1060	1141.4	2	109	
S (HT) §		956	1125.5	9	103.4	
O (HT) †		1229	1290	8	94	425
S (HT) †	900	945		18.8	94	360
SP (HT) †	634	795		20	97	310

*: From Brantley *et al.* (1996, 1998); §: From Morris (1989a); †: From product information literature.

Plus indicate that these room-temperature properties were not affected by the presence of boron in the alloy composition. Cracks perpendicular to the surface were observed for the heat-treated alloys (Fig. 12), and occasional horizontal cracks were observed in the near-surface oxidation region of Spartan Plus (Fig. 13). Figure 14 shows an aggregation of fine platelets and linear features in an apparently interdendritic region of a fractured as-cast Spartan Plus specimen, since this region contains a lamellar eutectic constituent (Brantley *et al.*, 1993). The morphology of these pronounced linear features suggest that they are crystallographically related. It is possible that they were formed by mechanical twinning processes.

Discussion

As previously noted, each alloy was melted in a separate ceramic crucible. The necessity of using a ceramic crucible for fusing high-palladium alloys has been demonstrated by Herø and Syverud (1985) and by van der Zel and Vrijhoef (1988), since very small amounts of carbon impurities from graphite crucibles decrease both ductility and metal-ceramic bond strength of these alloys.

The modulus of elasticity (E) is not significantly different for the three alloys in the two conditions. This result was expected, since E depends on bonding forces between atoms (Dieter, 1986) and the composition is very similar for these alloys. The absence of a significant effect of heat treatment on E confirms that the basic interatomic bonding, rather than microstructure, is the dominant factor. Variations in elastic modulus values shown in Table 2 are considered to arise from inherent accuracy limitations in the technique used to analyze the raw data.

For all three alloys, the significant decreases in YS and UTS after heat treatment might be due to the disappearance of hard secondary phases in the interdendritic areas and/or the transformation of incoherent to coherent precipitates which allow easier movement of dislocations and consequently increase ductility (percentage elongation) (Mohammed and Asgar, 1973). The present results concur with previous findings for Vickers hardness (Brantley *et al.*, 1996, 1998), where heat treatment significantly softened these three alloys compared to the as-cast condition (Table 3). However, in that study there were no significant differences among the mean hardness values of the three as-cast bench-cooled alloys. Additionally, there were no significant differences in the hardness of the three alloys after simulated porcelain firing. Lack of correlation between the tensile strength and Vickers hardness has been observed for Co-Cr and Ni-Cr alloys for removable prosthodontics (Bridgeport *et al.*, 1993).

The present data from the tension test thus reveal

differences in the mechanical properties of the three alloys that were not detected with the Vickers hardness test. Since all three alloys have very similar compositions and microstructures for the same condition, one may conjecture that the relatively higher yield strength of Spartan compared with Spartan Plus and Option might be caused by differences in orientation of the dendritic structure (perhaps affected by the boron content in the alloy). This might be an indication that the tension test results are more orientation-sensitive than the Vickers hardness test results.

The simplest way to assess the mechanical properties of alloys is by indentation hardness (Vander Voort, 1984). It has been shown that the Vickers hardness can be correlated with yield strength, but the correlations are material-dependent (Dieter, 1986). Although the indentation hardness is a practical test, fundamental studies of the mechanical behavior of metallic materials usually employ the tension test.

The mechanical properties of Spartan have been previously studied in tension (Morris, 1989a). Morris (1989a) also found that the YS and percentage elongation were significantly different for the as-cast and heat-treated conditions, whereas values of E and UTS did not change (Table 3). Comparing these results with Table 2, considerably higher mean values were obtained in our study for E in both conditions, UTS in the as-cast condition and percentage elongation in the heat-treated condition. Table 3 also shows that the values provided in the product information literature for YS, UTS and percentage elongation of Option, for YS of Spartan Plus, and E of all three alloys, are quite different from the results of this study.

The YS and UTS of Option were lower than for Spartan and at the same level as for Spartan Plus; the percentage elongation was similar for Option and Spartan Plus, and higher than Spartan (Table 2). According to the product information literature, the nominal compositions of Option and Spartan are the same. Both contain less than 1 wt% boron. It has been hypothesized that boron segregates at grain boundaries between the dendrites and interdendritic regions (SP Schaffer, Williams/Ivoclar, private communication). Due to the potentially deleterious effect of boron for the high-temperature creep of these alloys, this element was removed from Spartan to yield the alloy Spartan Plus (SP Schaffer, private communication). The inability to detect boron in Option and Spartan during a previous investigation was not surprising, because of the small concentration of this element and the possibility of its loss during fusion of the alloy (Brantley *et al.*, 1996, 1998). A plausible explanation (TB Cameron, Ney Dental, private communication) of the differences in mechanical properties may be that the manufacturers of Option (Ney Dental) and Spartan (Williams/Ivoclar) incorporate different amounts of boron in the alloy compositions.

The clinical importance of each mechanical property is not well established. In general, suitably high yield strength, high percentage elongation and medium hardness are desirable properties. Yield strength is considered to be more important than ultimate strength in clinical applications because a small amount of permanent deformation may cause the cast restoration to become clinically unacceptable. A high modulus of elasticity will not allow the restoration to bend substantially with application of forces and is an especially important property for metal-ceramic restorations. The strain-hardening exponent indicates the rate at which the alloy work hardens during permanent deformation, and the rate of work hardening is very important for the adjustment of clasps on removable partial dentures where some permanent deformation is necessary. The strain-hardening exponent has values that range from $n = 0$ for a perfectly plastic solid to $n = 1$ for a perfectly elastic solid (Dieter, 1986). It might be conjectured that a relatively low value of n would allow multiple adjustments of a removable partial denture clasp without considerable work hardening and potential fracture. This hypothesis is based upon previous studies where the rapidly work hardening base metal casting alloys for removable partial denture clasps have relatively low values of percentage elongation (Bridgeport *et al.*, 1993). Alloys that have high hardness are difficult to manipulate, both in the dental laboratory and during the chairside clinical procedures of adjustment and polishing. They also have the potential to wear the opposing natural dentition.

The present results for the microstructural changes after heat treatment agree with previous observations. Significant microstructural changes were observed for Spartan after simulated porcelain firing heat treatment (Brantley *et al.*, 1993; Carr *et al.*, 1993). The as-cast dendritic microstructure of Spartan was nearly eliminated, and new phases were observed. The same changes were subsequently observed for heat-treated Option and Spartan Plus (Brantley *et al.*, 1996, 1998).

Hot tears, which have been previously found in thin copings of Spartan (Carr *et al.*, 1993), were not observed in this study. Hot tears, which occur during solidification of the dendritic alloy, usually appear as long cracks at the boundaries between dendrites and interdendritic regions, and are sources of weakness in sites of high stress concentration for static loading or of fatigue fracture initiation for cyclic loading (Carr *et al.*, 1993). When the initially formed skeleton of the palladium solid solution dendrites is no longer able to move readily, it develops some strength as the temperature decreases. The increasing strength of the solid network can cause localized strains between the dendrites and the

subsequently freezing interdendritic areas, which should also shrink during solidification, resulting in the formation of cracks in thin areas of the casting (Flemings, 1974). The tension test specimens used in this study were much larger than the simulated clinical copings used by Carr *et al.* (1993). The cracks observed in the oxidation area of the failed specimens (Figs. 12 and 13) demonstrate the relatively weak and brittle nature of this region. It can be seen in Figure 12 that these cracks terminate at the boundary of the subsurface oxidation region and the adjacent denuded zone. Further research to determine the potential importance of this event for clinical metal-ceramic and all-metal restorations is needed.

The apparent observation of twinning in the interdendritic region of as-cast Spartan Plus (Fig. 14) is consistent with recent transmission electron microscopy (TEM) studies of high-palladium alloys by Cai (1996) who observed a twin boundary in an as-cast specimen of Pd-Ga alloy Legacy (J.F. Jelenko & Co., Armonk, NY). Nitta (1997) has found that the 100-200 nm wide bands in the ultrastructures of representative high-palladium alloys are caused by microtwinning. Twinning in the complex interdendritic regions of Spartan Plus (and presumably also Spartan and Option) is plausible because it provides a means of deformation where dislocation movement is difficult, as is expected in two or more intimately coexisting microstructural phases with different crystal structures. Future TEM studies of deformed high-palladium alloys are planned in our laboratory to elucidate the nature of dislocation interactions and strengthening mechanisms.

A small amount of porosity was found in the castings of all three alloys. This result is in accord with a previous study of a Pd-Ga alloy, where minimal porosity was found in specimens of similar size fabricated by induction melting and centrifugal casting (Stewart *et al.*, 1992). Therefore, it appears that torch melting of these high-palladium alloys for large patterns produces castings of acceptable quality. Induction melting has been considered as a more controlled means for casting alloys than torch melting (Morris, 1989b). The effect of the melting technique on the mechanical properties should be investigated further.

Conclusions

Under the conditions of this study, the following conclusions may be drawn:

(1). The alloys Option and Spartan Plus exhibited similar mechanical properties. Spartan had higher YS and UTS, and lower elongation, compared to Option and Spartan Plus.

(2). Heat treatment simulating the porcelain firing cycles eliminated the dendritic microstructure, decreased YS and UTS, and increased ductility for all three alloys.

(3). Use of the tension test revealed differences among the mechanical properties of the three alloys that were not observed previously by Vickers hardness testing.

Acknowledgments

The authors are grateful to Dr. Thomas B. Cameron of Ney Dental for helpful comments about the presence of boron in these alloys.

References

ADA (American Dental Association) Council on Dental Materials, Instruments and Equipment (1991) ANSI/ADA specification no. 38 for metal-ceramic systems. Chicago, IL.

ADA (American Dental Association) Council on Dental Materials, Instruments and Equipment (1996) ANSI/ADA specification no. 5 for dental casting alloys. Chicago, IL.

Asgar K (1988) Casting metals in dentistry: Past-present-future. Adv Dent Res **2**: 33-43.

Asgar K, Techow B, Allan FC, Sutfin LV (1969) Effect of casting conditions on physical properties of some experimental partial denture alloys. J Biomed Mater Res **3**: 409-423.

ASM International (1992) Tensile testing. Metals Park, OH. pp 49-60.

Brantley WA, Cai Z, Carr AB, Mitchell JC (1993) Metallurgical structures of as-cast and heat-treated high-palladium dental alloys. Cells Mater **3**: 103-114.

Brantley WA, Wu Q, Cai Z, Vermilyea SG, Mitchell JC (1996) Effects of casting conditions and annealing on dendritic Pd-Cu-Ga alloys. J Dent Res **75**: 60 (IADR Abstract No. 339).

Brantley WA, Wu Q, Cai Z, Vermilyea SG, Mitchell JC, Comerford MC (1999) Effects of casting conditions and annealing on microstructures and Vickers hardness of dendritic Pd-Cu-Ga dental alloys. Cells Mater **9**: 83-92.

Bridgeport DA, Brantley WA, Herman PF (1993) Cobalt-chromium and nickel-chromium alloys for removable prosthodontics, Part 1: Mechanical properties. J Prosthod **2**: 144-150.

Cai Z (1996) Metallurgical Structures, *in vitro* Corrosion Resistance and Biocompatibility of High-Palladium Dental Alloys. Ph.D. Dissertation. The Ohio State University, Columbus, OH.

Carr AB, Brantley WA (1991) New high-palladium casting alloys: Part 1. Overview and initial studies. Int J Prosthodont **4**: 265-275.

Carr AB, Cai Z, Brantley WA, Mitchell JC (1993) New high-palladium casting alloys: Part 2. Effects of heat treatment and burnout temperature. Int J Prosthodont **6**: 233-241.

Dieter GE (1986) Mechanical Metallurgy (3rd ed). McGraw-Hill, New York. pp. 254-256, 275-324 and 329-335.

Flemings MC (1974) Solidification Processing. McGraw-Hill, New York. pp. 253-256.

Herø H, Syverud M (1985) Carbon impurities and properties of some palladium alloys for ceramic veneering. Dent Mater **1**: 106-110.

Lausten LL, Luebke NH, Brantley WA (1993) Bending and metallurgical properties of rotary endodontic instruments. IV. Gates Glidden and Peeso drills. J Endodon **19**: 440-447.

Mohammed H, Asgar K (1973) A new dental superalloy system: I. Theory and alloy design. J Dent Res **52**: 136-144.

Morris HF (1989a) Veterans administration cooperative studies project no. 147/242. Part VII: The mechanical properties of metal ceramic alloys as cast and after simulated porcelain firing. J Prosthet Dent **61**: 160-169.

Morris HF (1989b) Veterans administration cooperative studies project no. 147. Part IX: A comparison of the mechanical properties of several alternative metal ceramic alloys cast in clinical and research laboratories. J Prosthet Dent **62**: 146-153.

Nitta S (1997) TEM Investigation of the Tweed Structure in High-Palladium Dental Alloys. MS Thesis. The Ohio State University, Columbus, OH.

Papazoglou E, Brantley WA, Carr AB, Johnston WM (1993) Porcelain adherence to high-palladium alloys. J Prosthet Dent **70**: 386-394.

Schaffer SP (1983) Novel palladium alloy and dental restorations utilizing same. US Patent 4,387,072.

Stewart RB, Gretz K, Brantley WA (1992) A new high-palladium alloy for implant-supported prostheses. J Dent Res **71**: 158 (AADR Abstract No. 423).

van der Zel JM, Vrijhoef MMA (1988) Carbon absorption of palladium-enriched ceramic alloys. J Oral Rehab **15**: 163-166.

Vander Voort GF (1984) Metallography: Principles and Practice. McGraw-Hill, New York. pp. 334-409, 410-508.

Vrijhoef MMA, Greener EH (1988) Some academic reflections on casting alloy patents. Dent Mater **4**: 313-317.

Discussion with Reviewers

M.D. Bagby: What is the basis in terms of data or references for the supposition that the differences in the strengths of the three alloys were caused by differences in orientation of the dendritic structure?

Authors: While we have speculated that the differences in mechanical properties of these alloys may arise from orientation variations in the dendritic structure, we consider a more plausible explanation is that these differences are due to variations in the amount of boron incorporated in the alloys by the manufacturers. However, we were unable to verify this latter hypothesis with our microprobe measurements.

H.J. Mueller: While fracture can be thought to have occurred due to two interpenetrating networks, the first consisting of ductile dendrites and the second consisting of the brittle interdendritic constituent, what fracture mode mostly characterized the relatively brittle alloys? Figure 3 reveals the apparent flat regions associated with brittle fracture. However, Figures 4 and 5 reveal that these regions are far from flat, but rather indicate fractured interfacial regions between dendrites and the hard Pd-Ga phase. Does any further evidence support either one of these fracture mechanisms over the other?

Authors: The overall fracture process in the as-cast alloys is a complex mixture of brittle and ductile fracture, whereas the alloys subjected to the simulated porcelain firing cycles undergo ductile fracture. Examination of the higher-magnification Figure 4 indicates that the "web-like" pattern of ridges in Figure 3 corresponds to the interdendritic regions. Further research is necessary to define the fracture processes occurring at the boundaries between the dendrites and the interdendritic regions.

H.J. Mueller: Figure 12 brings out the poor porcelain bonding potential to these alloys if cracks are easily formed in the outer oxide layer due to stress application. Although simulation of the porcelain firing procedures by subjecting alloys to the temperatures and times recommended by the manufacturers is useful, it should be emphasized that simulations are one step away from the actual porcelain firing. Heating an alloy with the actual porcelain brings out additional considerations not in effect during simulation procedures. For example, the alloy surface may not be exposed to or have the same affinity for oxygen as during simulation heating. Instead of forming a distinct thicker layer of oxide as during simulations, a thinner oxide layer chemically bonded to porcelain may instead occur during actual porcelain firings.

Authors: We concur with these comments and realize that study of fractured metal-ceramic test specimens is required to assess whether the same relatively brittle subsurface oxidation region will have an important role in fracture processes that may occur under clinical conditions. However, our previous SEM study of cross-sectioned metal-ceramic specimens (Papazoglou *et al.*, 1996) indicate that the near-surface regions of the alloys

after porcelain firing are very similar to those found after simulated porcelain-firing heat treatment (Brantley *et al.*, 1993). However, the external oxide formed on the high-palladium alloys was largely lost with the metallographic specimen preparation procedure used in the latter study. Subsequent examination of sectioned metal-ceramic specimens verified the anticipated reaction of this external oxide with the dental porcelain during the firing cycles.

H.J. Mueller: Your results show that the strain-hardening coefficient (n) is highest for the as-cast condition of the Spartan alloy. How may n be further improved to make these alloys more amenable to applications involving clasps for removable partial dentures?
Authors: Changes in the microstructure or ultrastructure of the alloys would be necessary to modify their work-hardening characteristics. Possible changes might be alteration of the type (coherent or incoherent) and size of precipitates that interact with dislocations during permanent deformation. A recent study in our laboratory of other high-palladium dental alloys having equiaxed fine-grained microstructures revealed a range of n similar to that in Table 2. More research is required to determine if innovative compositional changes or heat treatments can produce useful improvements in the work-hardening behavior of these palladium alloys.

Additional Reference

Papazoglou E, Brantley WA, Mitchell JC, Cai Z, Carr AB (1996) New high-palladium casting alloys: Studies of the interface with porcelain. Int J Prosthodont **9**: 315-322.